Acta Crystallographica Section D
Biological Crystallography
ISSN 0907-4449

The mammalian DUF59 protein Fam96a forms two distinct types of domain-swapped dimer

Kai-En Chen,[a] Ayanthi A. Richards,[b] Juliana K. Ariffin,[c] Ian L. Ross,[a,c] Matthew J. Sweet,[c,d] Stuart Kellie,[b,c,d] Bostjan Kobe[a,b,d] and Jennifer L. Martin[a,b]*

[a]Institute for Molecular Bioscience, Division of Chemistry and Structural Biology, University of Queensland, Brisbane, Queensland 4072, Australia, [b]School of Chemistry and Molecular Biosciences, University of Queensland, Brisbane, Queensland 4072, Australia, [c]Institute for Molecular Bioscience, Division of Molecular Genetics and Development, The University of Queensland, Brisbane, Queensland 4072, Australia, and [d]Australian Infectious Diseases Research Centre, Brisbane, Queensland 4072, Australia

Correspondence e-mail: j.martin@imb.uq.edu.au

Received 6 December 2011
Accepted 14 February 2012

PDB References: Fam96a, major dimer, 3ux2; Fam96a, minor dimer, 3ux3.

Fam96a mRNA, which encodes a mammalian DUF59 protein, is enriched in macrophages. Recombinant human Fam96a forms stable monomers and dimers in solution. Crystal structures of these two forms revealed that each adopts a distinct type of domain-swapped dimer, one of which is stabilized by zinc binding. Two hinge loops control Fam96a domain swapping; both are flexible and highly conserved, suggesting that domain swapping may be a common feature of eukaryotic but not bacterial DUF59 proteins. The derived monomer fold of Fam96a diverges from that of bacterial DUF59 counterparts in that the C-terminal region of Fam96a is much longer and is positioned on the opposite side of the N-terminal core fold. The putative metal-binding site of bacterial DUF59 proteins is not conserved in Fam96a, but Fam96a interacts tightly *in vitro* with Ciao1, the cytosolic iron-assembly protein. Moreover, Fam96a and Ciao1 can be co-immunoprecipitated, suggesting that the interaction also occurs *in vivo*. Although predicted to have a signal peptide, it is shown that Fam96a is cytoplasmic. The data reveal that eukaryotic DUF59 proteins share intriguing characteristics with amyloidogenic proteins.

1. Introduction

Over 3000 protein families containing a 'domain of unknown function' (DUF) have been classified in Pfam (Finn *et al.*, 2008). Proteins that contain the DUF59 domain exist in prokaryotes and eukaryotes, but the majority are found in bacteria and yeast. Several lines of evidence suggest a specific role for metal binding in DUF59 family members. Thus, in aerobic bacteria the two DUF59 proteins PaaD and PaaJ are metal-binding subunits of the phenylacetyl-coenzyme A oxygenase complex (Song *et al.*, 2006). Another study reported that the DUF59 domain-containing protein HCF101 is likely to be responsible for Fe–S cluster assembly in the model plant *Arabidopsis* (Lezhneva *et al.*, 2004). Moreover, sequence and structure analysis of the DUF59 protein TM0487 from *Thermotoga maritima* suggested a conserved metal-binding active site and a possible role for bacterial DUF59 proteins in binding Fe–S clusters (Macedo *et al.*, 2002; Almeida *et al.*, 2005).

Fam96a (family with sequence similarity 96 member A) is one of only two DUF59 proteins encoded in mammals. The other is Fam96b, also known as MIP18. The two Fam96 proteins share ∼50% sequence identity and differ in that Fam96a has a predicted signal sequence whereas Fam96b does

© 2012 International Union of Crystallography
Printed in Singapore – all rights reserved

not. Yeast two-hybrid (Y2H) data for Fam96a and Fam96b indicated that they may both interact with the protein Ciao1 (cytosolic iron–sulfur protein assembly 1; Rual *et al.*, 2005; Balk *et al.*, 2005). Recently, Fam96b and Ciao1 were shown to form part of the MMXD complex (MIP18–MMS19–XPD) with three other proteins [adenine nucleotide translocator 2 (ANT2), MMS19 nucleotide-excision repair protein homologue (MMS19) and the XPD transcription subunit; Ito *et al.*, 2010]. The MMXD complex is responsible for DNA repair and correct chromosome segregation (Ito *et al.*, 2010; Fan *et al.*, 2008). Knockdown of Fam96b in the human epithelial cell lines HCT116 and HeLa led to mis-localization of the mitotic spindle and an accumulation of abnormally shaped nuclei (Ito *et al.*, 2010). An additional function of Fam96b has recently been reported: in endothelial cells, Fam96b down-regulates the expression of the transcription factor E2-2. Since E2-2 negatively regulates the VEGF receptor 2 promoter, overexpression of Fam96b promotes endothelial cell migration and proliferation (Yang *et al.*, 2011). These data would therefore suggest that Fam96b is a positive regulator of angiogenesis.

Macrophages are key cellular regulators of innate immunity and also contribute to pathological processes in both acute and chronic inflammatory diseases. As such, macrophage-specific proteins are potentially important regulators of inflammation and could also prove useful as targets for anti-inflammatory design. Analysis of existing microarray data (http://biogps.org) indicated that mRNA expression of Fam96a was elevated in macrophages compared with other cell types and we therefore carried out a comprehensive structural and functional study of this protein.

Here, we confirm that *Fam96a* mRNA is enriched in macrophages and present *in vitro* and *in vivo* data validating a Fam96a–Ciao1 interaction. Crystal structure determination unexpectedly revealed that Fam96a forms two distinct domain-swapped dimers; there are tantalizing similarities to amyloidogenic proteins, which also form domain-swapped dimers.

2. Experimental procedures

2.1. Antibodies and constructs

Polyclonal anti-HA (H6908) antibody was obtained from Sigma–Aldrich. Anti-V5 monoclonal antibody (MCA1360) was obtained from AbD Serotec. Fam96a and Ciao1 for mammalian expression were amplified from murine macrophage cDNA and cloned into pEF6/V5-HisTOP (Invitrogen) in frame with a C-terminal C5 and His tag. A C-terminal HA tag was subsequently incorporated into Ciao1 by PCR amplification using the reverse primer 5′-TCAAGCGTAATCGCACATCGTATGGGTAGAGACCTGTGCAGGCTGGTG-3′.

2.2. Cell culture and transfection

Cell-culture and transfection reagents were obtained from Invitrogen. HeLa cells were maintained in Dulbecco's Modified Eagle's Medium (DMEM; 25 m*M* glucose) supplemented with 10% foetal bovine serum, 2 m*M* GlutaMAX I and non-essential amino acids and were transfected using Lipofectamine with Plus Reagent according to the manufacturer's protocols. Briefly, cells were seeded at 40–50% confluence onto glass cover slips in a 24-well plate. After 24 h, the wells were washed with OptiMEM reduced serum medium containing 2 m*M* GlutaMAX I and the medium was replaced with 0.5 ml of the same. A transfection mixture of 0.25 µg DNA and 1 µl Plus Reagent in 50 µl OptiMEM (per well) was prepared and incubated for 5 min at room temperature (RT) before combining with a mixture of 1 µl Lipofectamine in 50 µl OptiMEM (per well). After incubation for 25 min at RT to allow lipid-complex formation, the final mixture was added to the prepared cells. The medium was replaced with complete culture medium after 3 h and the cells were fixed after 8 h.

2.3. Immunofluorescence microscopy

Cells were fixed and processed for immunofluorescence microscopy as described previously (Richards *et al.*, 2002) with the following exceptions: fixation in 4% paraformaldehyde was followed by permeabilization in 0.1% Triton X-100 in phosphate-buffered saline (PBS) and the blocking solution was 0.5% bovine serum albumin in PBS. Experiments were viewed and imaged using either a Zeiss Axioplan 2 epifluorescent microscope or a Zeiss LSM 510 META confocal microscope and figures were prepared using *ImageJ*, *Adobe Photoshop* CS5.1 and *Adobe Illustrator* CS5.1 software.

2.4. Immunoprecipitation

Cells were harvested on ice into lysis buffer (50 m*M* HEPES, 150 m*M* NaCl, 1% Triton X-100, 1 m*M* Na_3VO_4, 30 m*M* NaF, 10 m*M* $Na_4P_2O_7$, 10 m*M* EDTA) containing a 1:25 dilution of protease-inhibitor cocktail (Sigma–Aldrich, catalogue No. P8340) and cleared (16 000*g* for 20 min at 277 K). Lysates were incubated overnight with 1 µg monoclonal anti-V5 before incubation for 4 h at 277 K with Protein G Agarose beads (Pierce) which had been blocked with 0.5% BSA in lysis buffer for 1 h at 277 K. The beads were washed four times in lysis buffer before the addition of DTT-containing sample buffer and boiling for 5 min. SDS–PAGE and Western blotting were performed as described previously (Richards *et al.*, 2006).

2.5. Topology determination: digitonin/trypsin method

Using a method adapted from a previous paper (Wunder *et al.*, 2010), transfected cells were washed twice in KHM buffer (110 m*M* potassium acetate, 20 m*M* HEPES pH 7.4, 2 m*M* $MgCl_2$) before treatment with 20 µ*M* digitonin in KHM buffer for 2 min at RT. Cells were then either washed once more in KHM buffer before harvesting of lysates ('digitonin only' condition) or further treated with 16 µ*M* trypsin–EDTA in KHM buffer for 2 min at RT and then harvested ('digitonin + trypsin' condition). Trypsin treatment was terminated by addition of serum-containing medium. Lysates were cleared and equal volumes were loaded for analysis by SDS–PAGE

and Western blotting for the epitope tags on the transfected proteins.

2.6. Topology determination: freeze–thaw method

Cells were seeded on glass cover slips, transfected and allowed to express for 8–9 h prior to topology determination by the method of Mardones & González (2003). Briefly, the cover slips were washed and quick-frozen by placing them cell-side up on a metal block pre-chilled in a 193 K freezer. After 10 s, the cover slips were transferred to another metal block pre-heated to 313 K for a further 10 s before fixation in 4% paraformaldehyde for 20 min at RT. The cells were subsequently permeabilized with 0.2% Triton X-100 in PBS for 15 min, or not permeabilized, before routine processing for immunofluorescence microscopy.

2.7. Quantitative real-time PCR

For primary cell populations, mouse T and B cells were purified from the spleens of C57BL/6 mice using MACS cell separation (Miltenyi Biotec) and CD90.2 and CD19 beads, respectively. Mouse macrophages (thioglycollate-elicited peritoneal macrophages) were generated from C57BL/6 mice. In brief, mice were administered (intraperitoneal injection) 1 ml sterile thioglycollate broth [10%(*w*/*v*) in H_2O]. After 5 d, elicited macrophages were harvested by peritoneal lavage. To generate human monocyte-derived macrophages (HMDMs), $CD14^+$ monocytes were purified from buffy coats using MACS CD14 positive selection kits (Miltenyi Biotec) and were cultured in the presence of 1×10^4 U ml^{-1} recombinant human CSF-1 (Chiron) for 7 d. For all cell populations shown, RNA was purified using the RNeasy Mini Kit (Qiagen) following the manufacturer's instructions. cDNA was synthesized from 1.25 µg total RNA using Superscript III Reverse Transcriptase (Invitrogen). The CT (cycle threshold) values of housekeeping control genes (*Hprt*, *Tbp*, *Cxxc1* and *Rpl13a* for mouse and *HPRT* and *TBP* for human) were averaged to obtain overall housekeeping gene CT values that were used to normalize *Fam96a* mRNA expression across the different cell populations.

2.8. Purification of Fam96a

Full-length human *FAM96A* was purchased from Open Biosystems and the construct that we used (residues 31–157) was cloned into the vector pMCSG7 (encoding an N-terminal His tag) by ligation-independent cloning (Stols *et al.*, 2002). His-tagged Fam96a was expressed in *Escherichia coli* BL21 (DE3) pLysS at 298 K for 24 h by autoinduction (Studier, 2005). Cell pellets were lysed in 150 ml (per litre of culture) lysis buffer consisting of 50 m*M* HEPES pH 7.5, 300 m*M* NaCl, 5 m*M* $MgCl_2$, 5% glycerol, 1% Triton X-100, 25 µg ml^{-1} DNase (Sigma–Aldrich) and 100 µl Protease Inhibitor Cocktail III (AG Scientific Inc.). Metal-affinity chromatography was performed using TALON cobalt resin (Clontech). The lysate was centrifuged at 20 000 rev min^{-1} for 30 min using a JA25.5 rotor in an Avanti J-25I centrifuge (Beckman Coulter) to separate soluble supernatant and insoluble cell pellet. Supernatant from the cell lysate was incubated with 4 ml resin for 2 h at 277 K with rotation. The resin was washed with 100 ml wash buffer consisting of 50 m*M* HEPES pH 7.5, 300 m*M* NaCl, 20 m*M* imidazole. His-tagged Fam96a was eluted with 50 m*M* HEPES pH 7.5, 300 m*M* NaCl, 300 m*M* imidazole.

Following metal-affinity purification, 1 mg tobacco etch virus (TEV) protease was added per 100 mg eluted protein to remove the His tag from Fam96a. The mixture was dialyzed for 48 h in 3500 Da molecular-weight cutoff membrane tubing (Pacific Laboratory) against 2 l dialysis buffer consisting of 50 m*M* HEPES, 300 m*M* NaCl, 5% glycerol, 2 m*M* fresh DTT at 277 K. After dialysis, cleaved and uncleaved proteins were separated using TALON resin. The flowthrough containing the His-tag-cleaved protein was collected and further purified by size-exclusion chromatography (SEC). The protein was eluted at 1 ml min^{-1} from a Superdex 75 16/60 column (Amersham Biosciences) equilibrated with SEC buffer (25 m*M* HEPES pH 7.5, 150 m*M* NaCl, 2 m*M* fresh DTT). The SEC column was calibrated with protein molecular-weight standards 12 000–200 000 Da (Sigma). Protein concentrations were measured using the Bradford assay (Bio-Rad).

To evaluate the effect of zinc on Fam96a, the purified monomer fraction was buffer-exchanged into 25 m*M* sodium acetate pH 5.0, 150 m*M* NaCl, 1 m*M* zinc acetate and incubated for 6 d at 277 K. After 1 and 6 d, the oligomeric state of the protein was analysed using a Superdex 75 16/60 column. At 6 d Fam96a had precipitated and was collected by centrifugation for 10 min at 4000 rev min^{-1}. Prior to SEC analysis using the same column the pellet was solubilized in 25 m*M* HEPES pH 7.5, 150 m*M* NaCl.

Seleno-DL-methionine-labelled Fam96a was expressed in minimal medium containing 100 µg seleno-DL-methionine (SeMet) per litre of culture using *E. coli* BL21 (DE3) strain at 298 K by IPTG induction, similar to the method described elsewhere (Edeling *et al.*, 2001). The purification of SeMet-labelled Fam96a followed the same procedure as used for the native protein.

2.9. Purification of Ciao1

Full-length human *CIAO1* was purchased from Open Biosystems and cloned into pMCSG7 using ligation-independent cloning (Stols *et al.*, 2002). Full-length His-tagged Ciao1 was expressed and purified as described for Fam96a. Purified Ciao1 was mixed with either dimeric or monomeric purified Fam96a. To separate unbound protein, the Ciao1–Fam96a mixtures were eluted on a Superdex 200 16/60 column (Amersham Biosciences) equilibrated with SEC buffer, with the major peak eluting at the volume expected for a monomer.

2.10. Site-directed mutagenesis

The mutants 85-PTVP-88-AAAA and 87-VP-88-AA were generated using the QuikChange site-directed mutagenesis protocol following the manufacturer's instructions (Stratagene). The Δ123–157 deletion mutant was cloned using primers designed to remove the C-terminal residues. The

mutants were transformed into *E. coli* BL21 (DE3) pLysS and expressed and purified following the same procedure as used for the native protein.

2.11. Crystal structure determination of Fam96a

Initial crystals of Fam96a major dimer were grown by hanging-drop vapour diffusion at 277 K from 1 µl protein solution at 30 mg ml^{-1} and 1 µl reservoir solution consisting of 50 m*M* HEPES pH 7.0, 200 m*M* ammonium sulfate, 30% polyethylene glycol (PEG) 3350. The best-quality crystals of the major dimer were obtained using a streak-seeding technique with serial dilution of protein concentration (Bergfors, 2003). Crystals grown at 30 mg ml^{-1} were used to seed the same condition containing 13 mg ml^{-1} protein. Initial crystals of Fam96a minor dimer were grown by hanging-drop vapour diffusion at 277 K from 1 µl protein solution at 33 mg ml^{-1} and 1 µl reservoir solution consisting of 50 m*M* sodium acetate pH 4.7, 0.1 *M* sodium malonate, 5% dimethyl sulfoxide (DMSO), 17% PEG 3350, 10 m*M* zinc acetate. The optimal crystals of the minor dimer were obtained by streak-seeding of crystals grown at 33 mg ml^{-1} into the same condition with 15 mg ml^{-1} protein. Minor-dimer crystals could not be generated when the zinc acetate was replaced by nickel sulfate, iron(II) acetate or magnesium sulfate, but could be grown in the presence of zinc sulfate.

Prior to data collection, the major dimer crystal (approximate dimensions of 0.2 × 0.1 × 0.02 mm) was soaked in cryoprotectant consisting of 50 m*M* HEPES pH 7.0, 200 m*M* ammonium sulfate, 30% PEG 3350, 10% glycerol and then flash-cooled in liquid nitrogen. The crystal of the minor dimer was soaked in cryoprotectant consisting of 50 m*M* sodium acetate pH 4.7, 0.1 *M* sodium malonate, 5% DMSO, 17% PEG 3350, 10 m*M* zinc acetate, 15% PEG 400. X-ray diffraction data were measured on the Australian Synchrotron MX2 beamline (ADSC Quantum 315r detector) at a temperature of 100 K and a wavelength of 0.9184 Å using the *Blu-Ice* software (McPhillips *et al.*, 2002). The data were indexed and integrated by *XDS* (Kabsch, 2010) and scaled using *SCALA* (Winn *et al.*, 2011). Phases for the major-dimer structure were determined by single-wavelength anomalous dispersion (SAD) methods using data measured from a SeMet Fam96a crystal in the range 20.0–1.8 Å; f' and f'' used for phasing were −0.8787 and 1.1389, respectively. The crystal was grown in the same way as the native crystals. Heavy-atom positions were determined by *SHELXC*/*D*/*E* (Sheldrick, 2010) and phases were generated by *Phaser* (McCoy *et al.*, 2007). Initial model building was performed using *ARP*/*wARP* (Morris *et al.*, 2003).

The minor-dimer structure was solved using data obtained from a crystal with approximate dimensions of 0.1 × 0.1 × 0.15 mm. The crystal was soaked in cryoprotectant consisting of 90 m*M* sodium acetate pH 4.7, 240 m*M* sodium malonate, 5.7% DMSO, 16% PEG 3350, 10 m*M* zinc acetate, 15% PEG 400. X-ray diffraction data were measured on the Australian Synchrotron MX2 beamline (ADSC Quantum 315r detector) at a temperature of 100 K and a wavelength of 0.9537 Å. Phases for the minor dimer were determined by molecular replacement with *Phaser* (McCoy *et al.*, 2007). Initially, we attempted to solve the structure using a 'closed' monomer structure modelled from the major dimer, but this did not result in any phasing solutions. Instead, the solution was found using an 'open' monomer from the major dimer with residues 58–61 deleted and allowing the two subunits to be fitted independently.

Structure refinement was performed using *PHENIX* (Adams *et al.*, 2010). Isotropic *B*-factor refinement was used and riding H atoms were included. For the minor dimer, anisotropic *B*-factor refinement was performed for the Zn atoms. Waters were added using the ordered solvent process with default parameters in *PHENIX* and were checked manually. In each round of refinement, the refined model was rebuilt manually using *Coot* (Emsley & Cowtan, 2004) with $F_o - F_c$ difference maps as a guide. The quality and geometry of the refined structures were evaluated by *MolProbity* (Chen *et al.*, 2010). Structure figures were made using *PyMOL* (DeLano, 2002) and structure comparison was performed using *DALI* (Holm & Rosenström, 2010).

Three zinc ions were observed in the minor-dimer crystal structure. One zinc ion has a trigonal bipyramidal coordination, forming equatorial interactions with the sulfurs of two Cys90 residues and the oxygen of a bound acetate. All three zincs were modelled with anisotropic *B* factors. In both molecules in the asymmetric unit of the minor-dimer structure the electron density for the loop comprising residues 73–76 was relatively poor, indicating that this region is flexible. Coordinates and structure factors have been deposited in the PDB (3ux2 for the major dimer; 3ux3 for the minor dimer).

2.12. Chemical cross-linking

Dimeric and monomeric forms of Fam96a isolated by SEC were concentrated to 5 mg ml^{-1}. For cross-linking, 5 µl of 10 m*M* bis-sulfosuccinimidyl suberate (BS3) cross-linker was mixed with 50 µl dimer and monomer separately. Once the BS3 cross-linker had been added, 12 µl of reaction sample was removed immediately and 4 µl of fresh 0.5 *M* ammonium carbonate was added to stop the reaction (time = 0; T_0). The step was repeated after 10 min (T_1) and after 1 h (T_2) of reaction. All samples were analyzed using SDS–PAGE.

2.13. Analytical ultracentrifugation

Sedimentation-equilibrium analytical ultracentrifugation was performed for purified monomeric and dimeric forms of Fam96a. Both samples were concentrated to 0.3 mg ml^{-1} in 25 m*M* HEPES pH 7.5, 150 m*M* NaCl, 2 m*M* DTT. For each experiment, the protein was loaded into two-channel quartz-window sedimentation-velocity cells in an XLI analytical ultracentrifuge (Beckman Coulter) using an SW60Ti rotor. Sedimentation-equilibrium data were recorded at 277 K at a speed of 18 000 rev min^{-1} (43 700*g*) as well as 42 000 rev min^{-1} (238 000*g*) to determine the baseline. Absorbance was monitored at 240 nm. *SEDNTERP* software (Alliance Protein Laboratory) was used to calculate the protein and buffer properties and the data were analysed using *SEDANAL*

(Stafford & Sherwood, 2004). The samples were run three times.

2.14. Isothermal titration calorimetry

Isothermal titration calorimetry (ITC) experiments were performed at 298 K using an ITC200 (Microcal). Fam96a and Ciao1 were purified by SEC in 25 m*M* HEPES pH 7.5, 150 m*M* NaCl, 2 m*M* DTT before the titrations. For thermodynamic characterization of the interaction of Fam96a and Ciao1, Fam96a monomer or dimer at 160–660 µ*M* was injected into a sample cell containing Ciao1 at 15–55 µ*M*. Each experiment involved 16 injections of 2.45 µl with a stirring speed of 1000 rev min^{-1} and a spacing period of 180 s between injections. The *c* values are higher than optimal (>1000) owing to limitations of the experimental setup; the binding affinity may not be accurate as a consequence of these limitations. Thermodynamic parameters including equilibrium constant K_a (=1/K_d), binding enthalpy (ΔH), Gibbs free energy (ΔG) and entropy change ($T\Delta S$) of the interactions were calculated from the heat of binding measured using *MicroCal Origin* 7.0 software (OriginLab). Stoichiometry (*N*) was refined initially and the value obtained was close to 1; after this, *N* was set to 1.0 for calculations. Thermodynamic parameters from three independent experiments were averaged to give the standard error of the mean (SEM).

3. Results

3.1. *Fam96a* mRNA is enriched in macrophages

Expression-profiling data for an extensive panel of mouse and human cell types has enabled the rapid mapping of tissue-specific gene-expression programmes (Su *et al.*, 2004; Wu *et al.*, 2009). We previously used this approach to identify macrophage-enriched GPCRs (Lattin *et al.*, 2008). These data also showed that *Fam96a* mRNA was expressed at elevated levels in mouse macrophage and related lineages compared with other cell types. To investigate the possible role of Fam96a in macrophages, we first confirmed that mRNA was expressed at elevated levels in this cell type. Quantitative real-time PCR analysis showed that *Fam96a* mRNA was expressed at higher levels in mouse macrophage cell lines (RAW264 and WR19M) compared with lymphoblast and fibroblast cell lines (Supplementary Fig. S1*a*[1]). Moreover, *Fam96a* mRNA expression in primary mouse macrophages was around fourfold higher than in primary B cells and T cells (Supplementary Fig. S1*b*[1]). *Fam96a* mRNA expression was similarly elevated in human monocyte-derived macrophages compared with a panel of human cell lines (Supplementary Fig. S1*c*[1]). Together, these data indicate that *Fam96a* mRNA is enriched in macrophages in both humans and mice, suggesting a potential role in macrophage biology and inflammatory pathways.

[1] Supplementary material has been deposited in the IUCr electronic archive (Reference: CB5007). Services for accessing this material are described at the back of the journal.

3.2. Fam96a forms stable monomers and dimers in solution

Size-exclusion chromatography (SEC) of purified recombinant human Fam96a lacking the N-terminal signal peptide

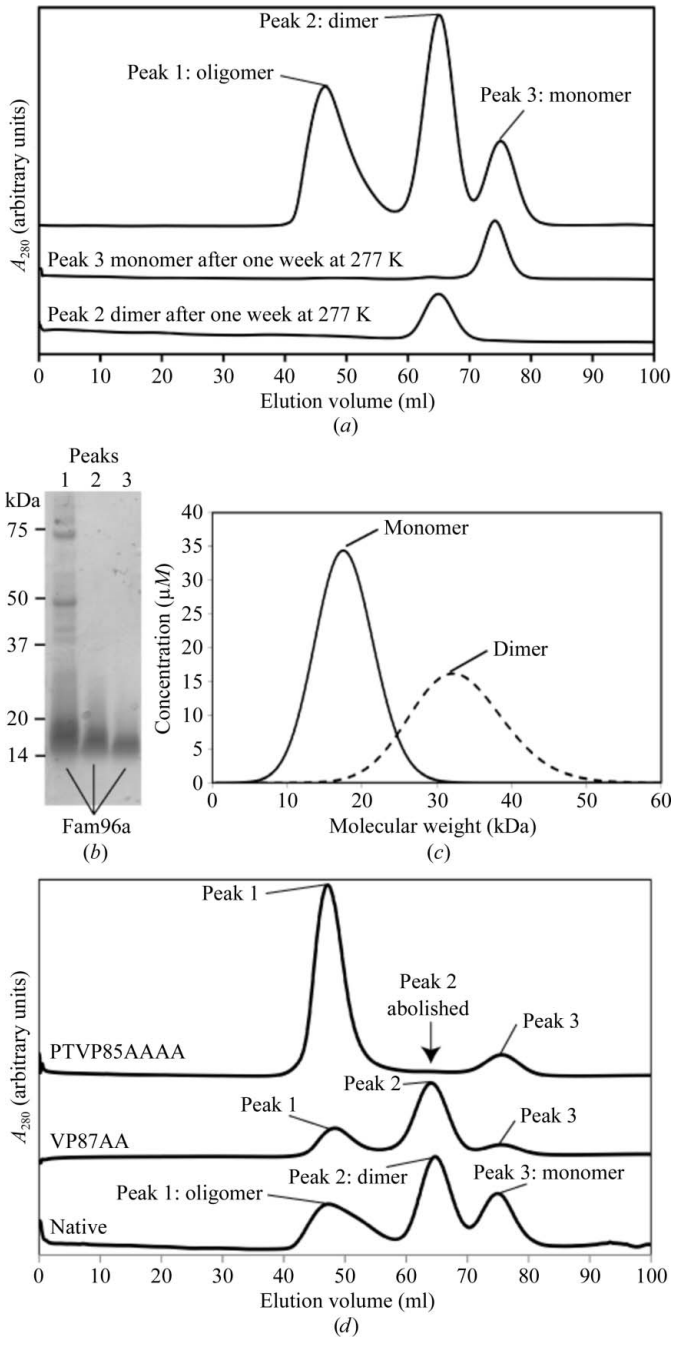

Figure 1
Oligomeric state of Fam96a. (*a*) Three distinct peaks elute from SEC of purified recombinant human Fam96a: peak 1, oligomer; peak 2, dimer; peak 3, monomer. The isolated monomer and dimer peaks remained stable for one week at 277 K. (*b*) SDS–PAGE of the three peaks: lanes 1, 2 and 3 contain oligomer, dimer and monomer, respectively. (*c*) Continuous size distributions determined by sedimentation-equilibrium analytical ultracentrifugation of monomeric (unbroken line) and dimeric (dashed line) Fam96a at 0.3 mg ml^{-1}. The image shown is representative of three scans. (*d*) The PTVP85AAAA mutant separated into two species on SEC consistent with oligomers and monomers. The VP87AA mutant separated into three species on SEC; as in native Fam96a, this is consistent with the formation of oligomers, dimers and monomers.

revealed three peaks, indicating the possibility of several oligomeric states (Figs. 1*a* and 1*b*). The first peak eluted in or near the void volume, suggesting the formation of large oligomers. SDS–PAGE analysis of this first peak revealed a ladder-like pattern (Fig. 1*b*), and this ladder was present whether or not 100 m*M* DTT reducing agent was used and whether or not the sample was boiled at 373 K for several minutes (not shown), suggesting that the peak comprises a mixture of higher order oligomers. The next peak eluted at a volume consistent with a Fam96a dimer and the third peak at a volume consistent with a Fam96a monomer. When the dimer and monomer peaks were separated and left for 7 d, no subsequent equilibration into two forms occurred, suggesting that the monomeric and dimeric forms are stable in solution under the conditions that we used and that there is an energetic barrier to conversion between the two forms (Fig. 1*a*). Analytical ultracentrifugation data showed that the purified monomer peak equilibrates at ∼15 kDa (consistent with a monomer) and the purified dimer peak equilibrates at ∼30 kDa (consistent with a dimer) (Fig. 1*c*). Chemical cross-linking with bis-sulfosuccinimidyl suberate (BS3) provides further support for the second peak representing a dimer (Supplementary Fig. S2*a*) and the third peak a monomer of Fam96a (Supplementary Fig. S2*b*). Taken together, the SEC, ultracentrifugation and cross-linking data suggest that Fam96a can exist in stable monomeric and dimeric forms in solution.

3.3. Fam96a interacts with Ciao1

Y2H data suggested that Fam96a and Fam96b can each form a complex with Ciao1 (Rual *et al.*, 2005), a 38 kDa protein responsible for iron–sulfur cluster-protein assembly in the cytoplasm and nucleus (Sharma *et al.*, 2010; Balk *et al.*, 2005). We analysed the interaction between purified forms of Fam96a and Ciao1 using isothermal titration calorimetry. We found that both the monomeric and dimeric forms of Fam96a interact with full-length Ciao1 with similar dissociation constants in the nanomolar range (Table 1; Supplementary Fig. S3). The binding-affinity values for Ciao1 of the Fam96a monomer and dimer are similar and they interact with one and two molecules of Ciao1, respectively.

We then examined the possibility of an interaction between Fam96a and Ciao1 in cells. HeLa cells were transiently co-transfected with Fam96a-V5 and Ciao1-HA or Ciao1-HA alone and the lysates were immunoprecipitated with monoclonal anti-V5 antibody. Equal volumes of starting material and immunoprecipitate were analysed by SDS–PAGE under reducing conditions followed by Western blotting for HA and V5. Co-immunoprecipitation of Ciao1-HA with Fam96a-V5 was reproducibly observed (Fig. 2*a*). The interaction was dependent on Fam96a, as Ciao1-HA did not bind to the beads in the absence of Fam96a-V5

Table 1
Thermodynamic parameters for Fam96a–Ciao1 interactions.

At least three replicate experiments were performed in each case. Values are expressed as mean ± standard error of the mean for three independent experiments. 1 cal = 4.186 J.

Ciao1	Fam96a	ΔH (kcal mol^{-1})	ΔG (kcal mol^{-1})	K_d (n*M*)	*N*
Ciao1	Monomer	−6.8 ± 0.4	−10.7 ± 0.4	18 ± 9.3	1.0
Ciao1	Dimer	−6.9 ± 0.7	−11.2 ± 0.6	11 ± 4.5	1.0

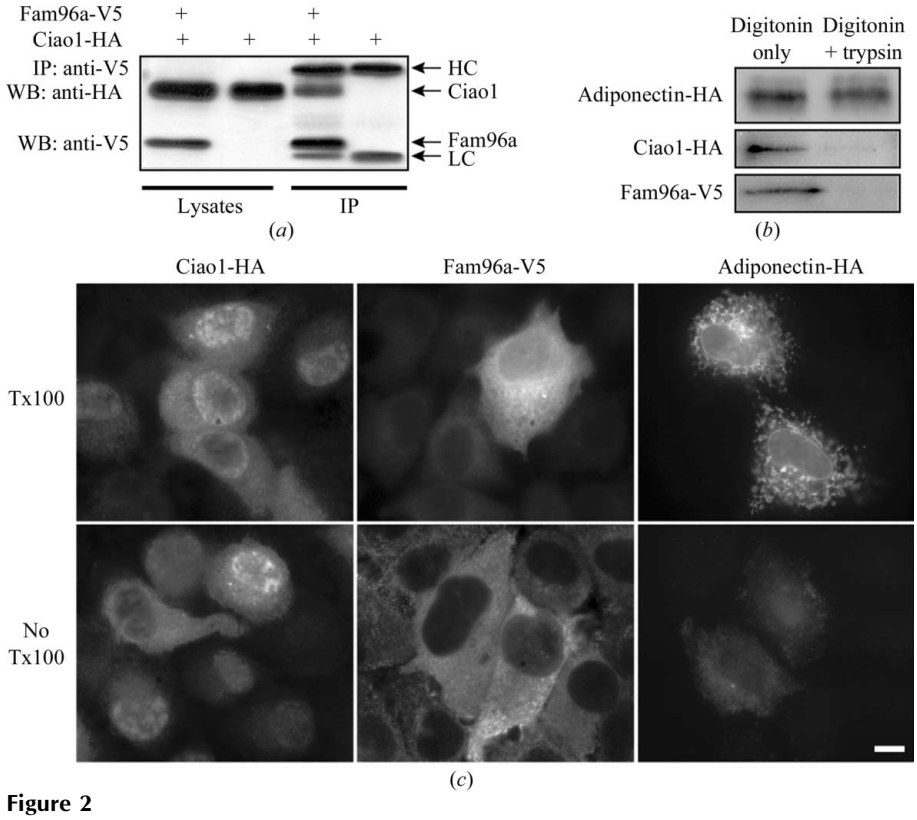

Figure 2
Fam96a co-immunoprecipitation and topology determination in HeLa cells. (*a*) HeLa cells were transiently co-transfected with either Fam96a-V5 and Ciao1-HA or Ciao1-HA alone. SDS–PAGE and Western blotting of lysates and immunoprecipitates (IP) revealed co-immunoprecipitation of Ciao1-HA with Fam96a-V5. No immunoprecipitation of Ciao1 was observed in the absence of Fam96a-V5. LC, IgG light chain. HC, IgG heavy chain. (*b*) Transfected HeLa cells expressing either adiponectin-HA, Ciao1-HA or Fam96a-V5 were treated with digitonin to selectively permeabilize their plasma membranes. While adiponectin-HA was largely protected from protease digestion following digitonin treatment, Ciao1-HA and Fam96a were clearly susceptible to proteolysis. The data shown are representative of three or more independent experiments. (*c*) Transfected HeLa cells expressing either adiponectin-HA, Ciao1-HA or Fam96a-V5 were subjected to one freeze–thaw cycle to selectively disrupt their plasma membranes before fixation and immunofluorescent labelling with or without Triton X-100 detergent permeabilization (Tx100 or No Tx100, respectively). Adiponectin-HA was brightly labelled after detergent permeabilization but poorly detectable in the absence of detergent treatment. Both Ciao1 and Fam96a were brightly labelled in both detergent-treated and untreated cells. Scale bar, 5 µm.

Table 2
Data-collection and refinement statistics of Fam96a crystal structures.

Values in parentheses are for the highest resolution shell.

	Major dimer, SeMet	Minor dimer
Data-collection statistics		
Wavelength	0.9184	0.9537
Space group	$C222_1$	$P2_1$
Resolution range (Å)	20–1.80 (1.90–1.80)	34–1.80 (1.86–1.80)
Unit-cell parameters (Å, °)	a = 76.4, b = 90.9, c = 34.7, $\alpha = \beta = \gamma = 90$	a = 49.2, b = 52.3, c = 65.9, $\alpha = \gamma = 90$, $\beta = 104.6$
Total observations	160221	204506
No. of unique reflections	11601 (1659)	30039 (2992)
Completeness (%)	99.9 (100)	99.6 (100)
$R_{\rm merge}$†	0.06 (0.23)	0.08 (0.51)
$\langle I/\sigma(I)\rangle$	33.9 (15.5)	18.1 (2.8)
Multiplicity	13.8 (14.1)	6.8 (7.2)
Phasing statistics		
Overall phasing power	1.11	
No. of selenium sites	2	—
FOM (overall/centric/acentric)	0.53/0.32/0.57	—
Refinement statistics		
Resolution range (Å)	19.54–1.80 (1.98–1.80)	34.24–1.80 (1.86–1.80)
No. of reflections used ($R_{\rm work}/R_{\rm free}$)	11035/554	28474/1523
$R_{\rm work}$‡/$R_{\rm free}$§ (%)	17.2/20.8	19.6/23.4
No. of atoms		
Protein	1139	2353
Water	128	177
Other	2 Se	3 Zn^{2+}, 1 acetate
Wilson B factor (Å^2)	14.0	24.3
Average B factor¶ (Å^2)		
Protein	16.3	36.9
Water	26.4	49.4
Zinc	—	38.2
R.m.s.d. isotropic B (main chain/side chain)	1.78/3.54	2.59/5.96
R.m.s.d. ideal values		
Bond length (Å)	0.007	0.006
Bond angles (°)	1.1	0.95
Ramachandran plot (%)		
Favoured	100	100
Allowed	96.3	99.3††

† $R_{\rm merge} = \sum_{hkl}\sum_i |I_i(hkl) - \langle I(hkl)\rangle| / \sum_{hkl}\sum_i I_i(hkl)$, where $I_i(hkl)$ is the intensity of the ith observation of reflection hkl. ‡ $R_{\rm work} = \sum_{hkl} ||F_{\rm obs}| - |F_{\rm calc}|| / \sum_{hkl} |F_{\rm obs}|$, where $F_{\rm obs}$ and $F_{\rm calc}$ are the observed and calculated structure-factor amplitudes for reflection hkl. § $R_{\rm free}$ was calculated using 5% of the diffraction data selected randomly and excluded from refinement. ¶ Calculated using *BAVERAGE* (Winn *et al.*, 2011). †† Two outliers: Asn73 from each of the two molecules in the asymmetric unit. This residue is located in a flexible loop.

(Fig. 2*a*). The interaction of Fam96a with the cytoplasmic/nuclear protein Ciao1 suggests a cytoplasmic rather than a lumenal distribution for Fam96a, despite a predicted N-terminal signal peptide. We therefore proceeded to experimentally determine whether Fam96a is in the cytoplasmic or the lumenal compartment.

Two independent methods were used to investigate Fam96a compartmentalization. The first involved selective permeabilization of the plasma membrane using digitonin followed by trypsin digestion and Western blotting for the C-terminal V5 tag of Fam96a-V5. An endoplasmic reticulum (ER) lumenal secreted protein, adiponectin-HA, was used as a control to ensure that lumenal epitopes were protected from protease treatment, and Ciao1-HA was used as a cytoplasmic positive control. As shown in Fig. 2(*b*), Fam96a and Ciao1 were susceptible to trypsin digestion whilst adiponectin-HA was protected, indicating that the C-terminal region of Fam96a is cytoplasmic.

In the second approach, transfected cells expressing either Fam96a-V5 or adiponectin-HA were subjected to a rapid freeze–thaw cycle (to selectively rupture the plasma membrane) before fixation and immunofluorescent labelling with or without prior detergent permeabilization. Adiponectin-HA was poorly detectable in the absence of detergent, as expected for a lumenal protein, while there was no difference in the brightness of labelled Fam96a-V5 with or without detergent (Fig. 2*c*). In summary, these results showed that the Ciao-1-interacting region of Fam96a is cytosolic, not lumenal.

3.4. Fam96a crystal structures reveal two types of domain-swapped dimers

We solved the crystal structure of the Fam96a dimer at 1.8 Å resolution. Unexpectedly, the protein formed a domain-swapped dimer across a crystallographic twofold axis (Fig. 3*a*, Table 2). Each subunit has an open conformation comprising five α-helices and two β-strands. The swapped portion of the structure is located in the middle of the polypeptide chain, with helix 3 interacting with helices 4 and 5 of an adjacent symmetry molecule. The hinge-loop regions that control the swapping are the proline-rich loop 84-TPTVPH-89 and the seven-residue loop 121-GTHSTEE-127. Mutation of the first hinge residues 85-PTVP-88 to AAAA changed the oligomerization state of the protein in that only monomer and oligomer formed (Fig. 1*d*). Mutation of 87-VP-88 to AA did not affect the oligomerization pattern, yielding all three forms observed for the wild-type protein (Fig. 1*d*). These results suggested that the PTVP region may be important for domain-swapped dimer formation, although only one of the proline residues may be necessary for this to occur.

The second hinge loop is located C-terminal to the swapped region and has no associated electron density in the experimental map, indicating that it is highly flexible. Such flexible loops are common in domain-swapped dimer structures (Schlunegger *et al.*, 1997; O'Neill *et al.*, 2006). The lack of density for this region means that there are two possible ways to connect the polypeptide chain in this crystal form (Fig. 3*b*). Automated modelling of the flexible loop using *ARP*/*wARP* selected the mode 1 connection (Fig. 3*a*, Supplementary Fig. S4). In the second possible connection mode (mode 2) the entire C-terminal half of the structure would be domain-swapped (Fig. 3*b*). The *ARP*/*wARP* approach uses PDB-derived structural data as driving parameters to select the more likely mode (Joosten *et al.*, 2008; Langer *et al.*, 2008), but

we cannot rule out the possibility that Fam96a may form mode 2 or both mode 1 and mode 2 connections.

The structure of Fam96a obtained from a crystal of the monomeric protein was also solved at 1.8 Å resolution. Surprisingly, the crystal structure of Fam96a revealed a second type of domain-swapped dimer (Fig. 4*a*, Table 2), which we designate the 'minor dimer' as opposed to the 'major dimer' described above. The two distinct types of domain-swapped dimer place Fam96a in the quasi-three-dimensional domain-swapped protein class (Liu & Eisenberg, 2002). In the minor dimer there are two molecules in the asymmetric unit and these are very similar to each other (r.m.s.d. of 0.37 Å for 130 C^{α} atoms). Comparison of the major- and minor-dimer structures shows they have the same secondary-structure arrangement apart from the two hinge regions. The first hinge, which is extended in the major dimer (Fig. 5*a*), forms a tight turn in the minor dimer connecting β2 and α3 (Fig. 5*b*). The second hinge (residues 122-THSTEE-127) is disordered in the major dimer (Fig. 5*c*). This hinge defines the swapped portion of the minor dimer, forming a β-strand that interacts with the equivalent β-strand from the second subunit (Figs. 4*b* and 5*d*). Intriguingly, removal of residues 123–157 resulted in Fam96a that formed larger oligomers only; no dimer or monomer eluted from SEC (data not shown). This suggests that the C-terminal region is important for stable monomer and dimer formation.

Zinc was necessary for crystallization of the minor dimer, and fluorescence excitation of the minor-dimer crystal gave a strong peak at 8636 eV consistent with Zn *K*α emission (data not shown). Addition of zinc to the purified monomer solution, followed by incubation for a week, resulted in precipitation of Fam96a; after redissolving in buffer the protein had formed dimers and oligomers, with little monomer remaining, as indicated by SEC (Supplementary Fig. S5). Three zinc ions were observed in the minor-dimer crystal structure. One zinc ion has a trigonal bipyramidal coordination, forming equatorial interactions with the sulfurs of two Cys90 residues and the oxygen of a bound acetate. The two axial ligands are the hydroxyls of two Ser124 residues in the dimer, but the zinc cannot coordinate both hydroxyls at once owing to the geometrical constraints of the site. Difference electron density suggested disorder of the zinc ion along this axial direction. All three zinc ions were modelled with anisotropic *B* factors.

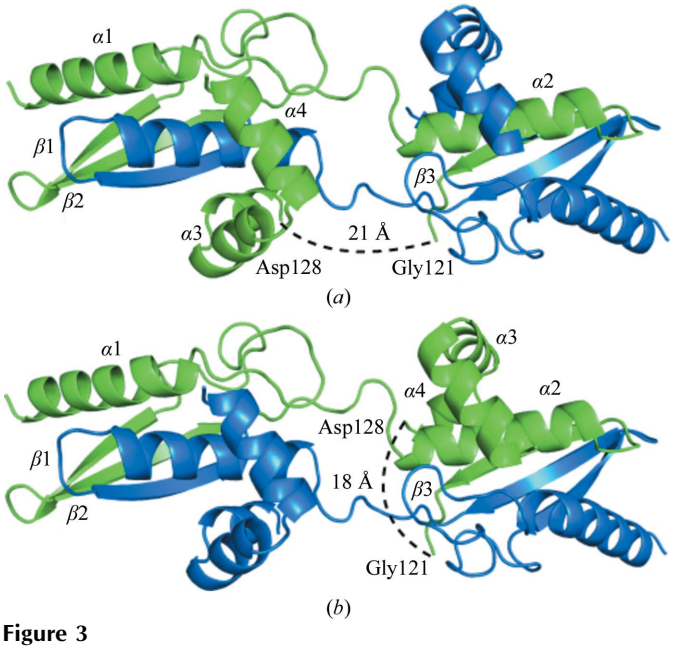

Figure 3
Structure of the Fam96a major dimer. (*a*) Cartoon representation of the Fam96a domain-swapped major dimer (mode 1 connection) with the protomers of the dimer shown in green and blue. (*b*) Mode 2 connection. The two possible linkages for hinge 2 (not modelled in the crystal structure) are indicated by dotted lines.

Interestingly, the zinc ligand Cys90 is located just after the first hinge loop and Ser124 is part of the second hinge-loop β-strand. The side-chain hydroxyl of a third residue, Thr122, also part of the second hinge-loop β-strand, is ∼3 Å from the sulfur of Cys90. Thus, the zinc ion coordinates residues from both hinge loops of both molecules in the domain-swapped dimer (Fig. 4*c*), supporting the notion that zinc may act as a switch between the monomer and minor-dimer forms. The other two zinc ions have a tetrahedral arrangement: each coordinates His89 and His123 of one monomer in the asymmetric unit and Glu150 and GluE153 from a symmetry-related molecule (Fig. 4*d*). His89 and His123 are also located on the two hinge loops. Significantly, His89, Cys90, Thr122 and His123 are highly conserved within the Fam96 family of proteins, but Ser124 is not (Supplementary Fig. S6). This leaves open the question of whether zinc binding and minor-dimer domain swapping is a common feature of the Fam96a/Fam96b/MIP18 family proteins or whether it occurs only in Fam96a proteins.

The structural differences between the two domain-swapped dimers of Fam96a are summarized in Table 3 and Fig. 6. The hinge-loop sequences are highly conserved in Fam96b/MIP18 family proteins (Supplementary Fig. S6), suggesting that hinge-loop flexibility and major-dimer domain-swapping is a conserved feature of eukaryotic DUF59-containing proteins.

4. Discussion

The structures of three bacterial DUF59 family protein structures have been solved [PDB entries 1uwd (Almeida *et al.*, 2005), 3lno (Center for Structural Genomics of Infectious Diseases, unpublished work) and 3cq1 (RIKEN Structural Genomics/Proteomics Initiative, unpublished work); Supplementary Table S1]. All three are monomers and feature a putative metal-binding site comprising Asp, Glu, Leu, Thr, Thr/Ser and Cys residues (Almeida *et al.*, 2005). The equivalent residues in mammalian Fam96a are Asp49, Glu51, Lys52, Thr86, Val87 and Cys90, *i.e.* two of the residues are not conserved in Fam96a. The hydrophobic Leu is proposed to contribute to a perturbed pK_a for the two acidic residues, which are relatively buried with no basic residues nearby (Almeida *et al.*, 2005). However, this Leu is replaced by the basic residue Lys52 in Fam96a and is either a Lys or a His in

other eukaryotic DUF59 proteins (Supplementary Fig. S6), ruling out this possibility in the eukaryotic proteins. In addition, the Thr/Ser of the cluster is replaced by Val87 in Fam96a and is either a Val or an Ile in other eukaryotic DUF59 proteins. Thus, the putative conserved metal-binding site of bacterial DUF59 proteins is not conserved in Fam96a or Fam96b.

A model of monomeric Fam96a generated by linking the two halves of a Fam96a minor dimer at residue His123 was compared with the structure of *Bacillus anthracis* DUF59 protein (PDB entry 3lno), which is representative of all three bacterial DUF59 protein structures (Fig. 7). This comparison revealed significant differences between the bacterial and mammalian DUF59 protein structures. Most notably, the region C-terminal to the second hinge loop is much longer in Fam96a than in the bacterial proteins (~35 compared with 15–20 residues). Strikingly, the helices formed from these residues in both the major and minor dimers of Fam96a are located on the opposite side of the core fold with respect to the same region of the bacterial DUF59 proteins (Fig. 7). This difference may be a consequence of the residues following strand $\beta3$ and preceding the second hinge loop of Fam96a; the mammalian proteins all have a Gly (Gly121) at this point, whereas the bacterial proteins have a Pro-Pro motif (Supplementary Fig. S6). This region appears to be the business end of the molecule in bacterial and mammalian proteins: domain swapping occurs here, zinc ions are bound at this end of the molecule and the putative metal-binding site of bacterial DUF59 proteins is located here. Nevertheless, if the bacterial and mammalian proteins did evolve from a common ancestor then their sequences and structures, and presumably their functions, have diverged remarkably, even aside from the issue of domain swapping.

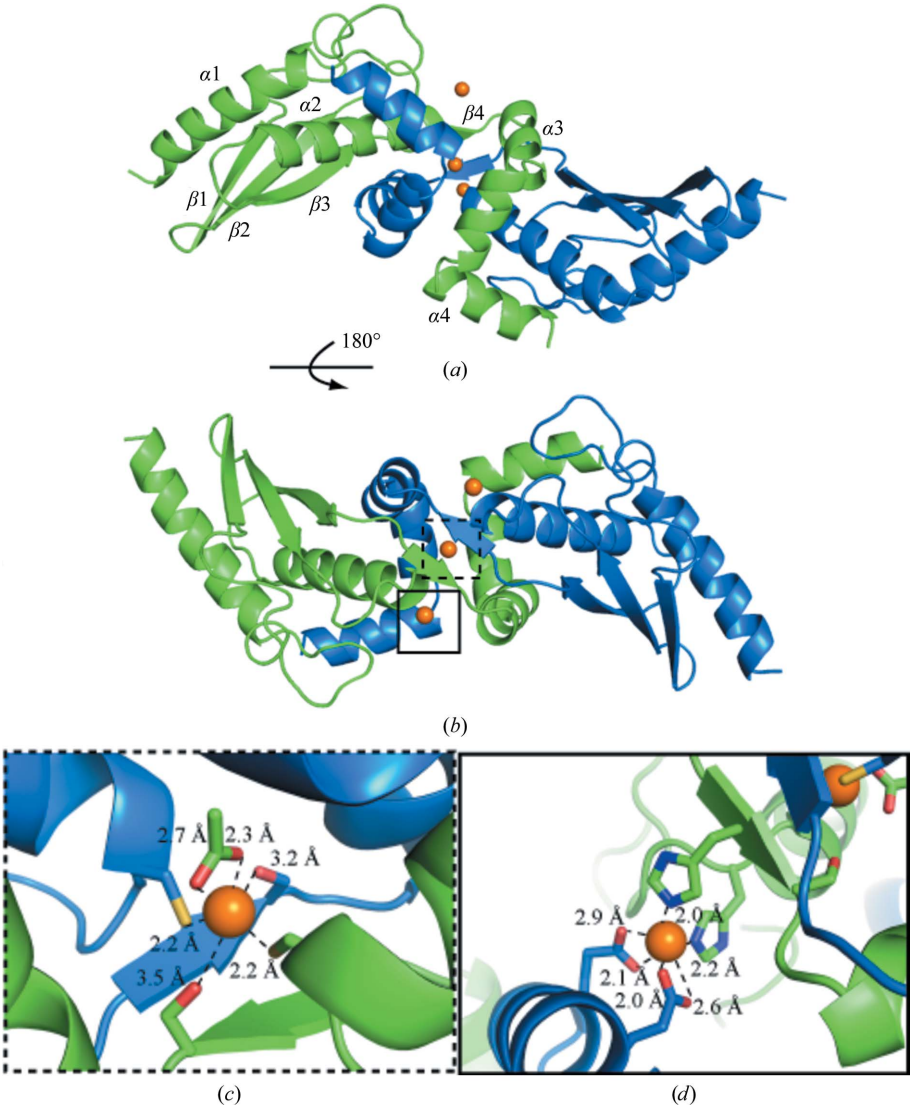

Figure 4
Structure of the Fam96a minor dimer. (*a*) Cartoon representation of the minor dimer (left-hand protomer shown in the same orientation as in Fig. 3*a*) and (*b*) rotated to show the central short β-sheet formed by hinge 2. Bound zinc ions are shown in orange. (*c*) Enlarged view looking into the zinc-binding site in the centre of the swapped dimer, showing the protein and acetate ligands. (*d*) Enlarged view looking into the zinc-binding site at the edge of the dimer.

Both Y2H data (Rual *et al.*, 2005; Srinivasan *et al.*, 2007) and co-immunoprecipitation analysis (Ito *et al.*, 2010) imply that Fam96b and Ciao1 interact within cells. We investigated a putative interaction between Fam96a and Ciao1 directly and found that these two proteins do indeed interact tightly *in vitro* and can be co-immunoprecipitated from cells. Compartmentalization experiments showed that Fam96a is cytoplasmic, in agreement with its interaction with a cytoplasmic protein. Although biological functions have been described for Fam96b (Ito *et al.*, 2010; Yang *et al.*, 2011), these functions are probably not conserved in Fam96a. For example, *Fam96b* mRNA is ubiquitously expressed (http://biogps.org), whilst our data demonstrate that *Fam96a* mRNA is expressed at elevated levels in macrophages. It is therefore possible that Fam96a has evolved an immune-related function which is distinct from that of Fam96b. We are currently investigating this possibility by focusing on potential functions for Fam96a in macrophages.

The finding that Fam96a forms two distinct types of domain-swapped dimer was unexpected given that the structures of three bacterial DUF59 proteins had been solved showing these to be monomers. Sequence analysis shows that the regions involved in domain swapping are well conserved in the eukaryotic DUF59 proteins, so that

Table 3
Comparison of the major and minor dimers of Fam96a.

Domain-swapped dimer	Major dimer, mode 1	Major dimer, mode 2	Minor dimer
No. of residues per molecule	127	127	127
Residues in hinge loop(s)	Thr84–His89 and Thr122–Glu127	Thr84–His89	Thr122–Glu127
No. of residues in swapped domain†	32	68	30
Location of swapped domain	Middle, α3 and β3	C-terminal, α3–α5	C-terminal, α4 and α5
Total molecular surface per dimer‡ (Å^2)	16434	16434	13349

† Counted from the first residue after the hinge loop. ‡ Total surface area calculated using *PISA* in the *CCP*4 program suite (Winn *et al.*, 2011).

domain swapping is likely to occur in those proteins but is unlikely in bacterial homologues, in which these regions are not conserved.

Protein domain swapping has been suggested to have several possible biological functions. For example, it has been proposed that the differing structural arrangements available to a protein through domain swapping (Fig. 6) may enable globular proteins to form repetitive oligomers that interact cooperatively with structurally repetitive molecules such as nucleic acids and oligosaccharides (Wouters *et al.*, 2010). It may also act as a means of switching a protein between different states of activity (Wouters *et al.*, 2010). There is no evidence that Fam96a binds nucleic acids or oligosaccharides and we found no difference in Ciao1 binding affinity for the monomeric and major-dimer forms of Fam96a. This suggests that if domain swapping does switch Fam96a on or off, this may involve minor-dimer formation or a function additional to binding Ciao1.

Many domain-swapped dimer proteins, including human prion protein (Zahn *et al.*, 2000; Knaus *et al.*, 2001; Lee & Eisenberg, 2003), cystatin C (Janowski *et al.*, 2004; Nilsson *et al.*, 2004; Janowski *et al.*, 2001) and β_2-microglobulin (Eakin *et al.*, 2004; Liu *et al.*, 2011), are amyloidogenic. A relatively common feature of amyloid-forming proteins is the formation of a β-strand in the hinge loop (Bennett *et al.*, 2006). Curiously, a β-strand occurs in the second hinge loop of the Fam96a minor dimer and this structure is stabilized by coordination to zinc, a metal linked to amyloid-plaque formation in neurodegenerative diseases (Zatta *et al.*, 2009). Intriguingly, amyloid-fibril formation can occur for stefin proteins in the presence of metal ions, which may reflect an interaction between the protein and biological surfaces (Žerovnik *et al.*, 2011). Redox processes have also been implicated in amyloid formation and

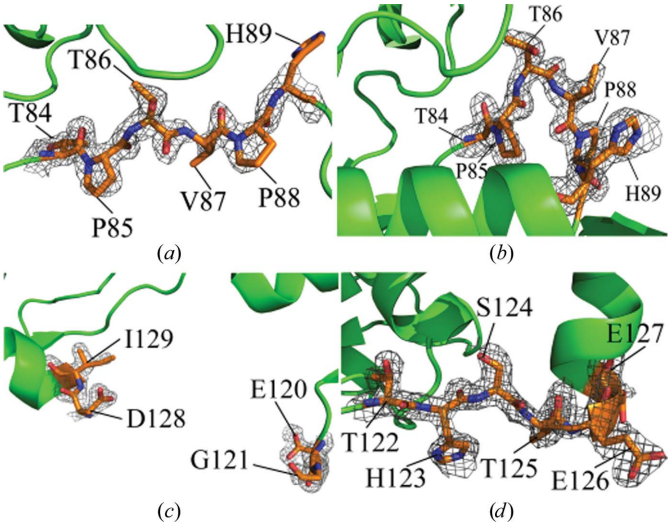

Figure 5
Fam96a hinge-loop analysis. (*a*) Major dimer and (*b*) minor dimer hinge loop 1 and (*c*) major dimer; (*d*) minor dimer hinge loop 2 (shown in orange). The electron density in (*a*), (*b*) and (*d*) corresponds to simulated-annealing OMIT $F_o - F_c$ maps contoured at 2.5σ.

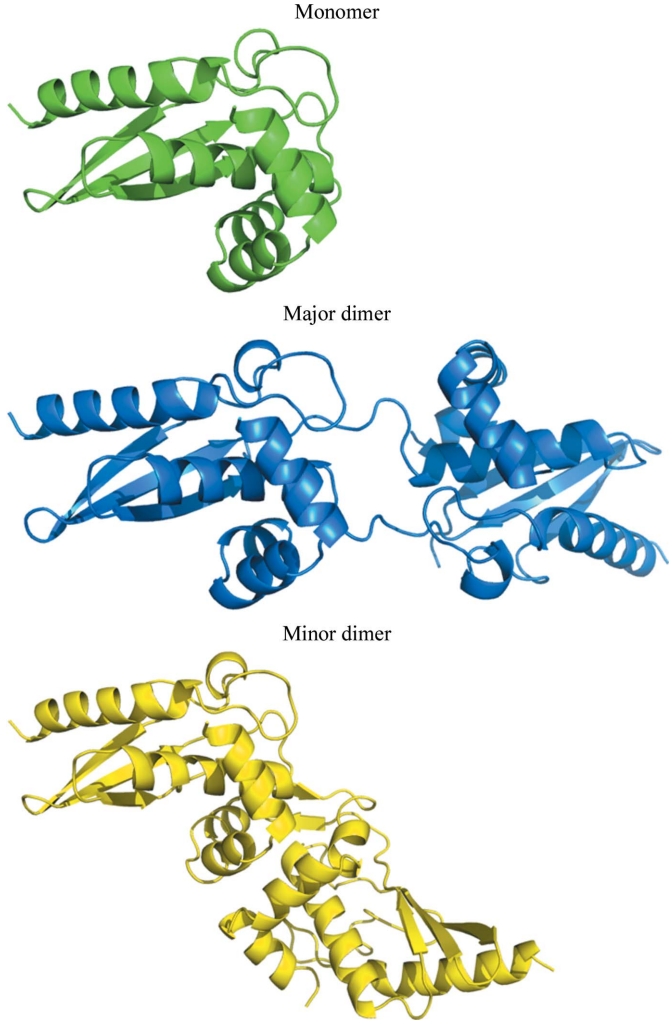

Figure 6
Structural arrangements of Fam96a. The model of the monomer (green; derived from the domain-swapped minor-dimer structure) and crystal structures of the major dimer (blue) and minor dimer (yellow) highlight three of the different structural arrangements that are potentially available to Fam96a.

a possible three-way relationship between redox-active cysteines, domain swapping and amyloid-forming proteins has been noted (Wouters *et al.*, 2010). There is certainly potential for the two Cys90 residues of Fam96a to form a disulfide across the minor dimer in the absence of zinc. This cysteine is highly conserved across DUF59 proteins (Supplementary Fig. S6). Moreover, the sulfurs of Cys99 (protomer *A*) and Cys155 (protomer *B*, and *vice versa*) are located near each other (∼4 Å) and could form a disulfide under the right conditions. The electron-density map shows no evidence of a disulfide (Supplementary Fig. S7) and the Fam96a SEC oligomerization pattern did not change when 2 m*M* fresh DTT was added to the buffer (not shown). This suggests that disulfide-bond formation does not occur in Fam96a under the conditions we used and it is certainly not essential for domain-swapped dimer formation. Whether the ability of Fam96a to bind zinc and form disulfides plays a role in amyloid-fibre formation will be an interesting question for the future.

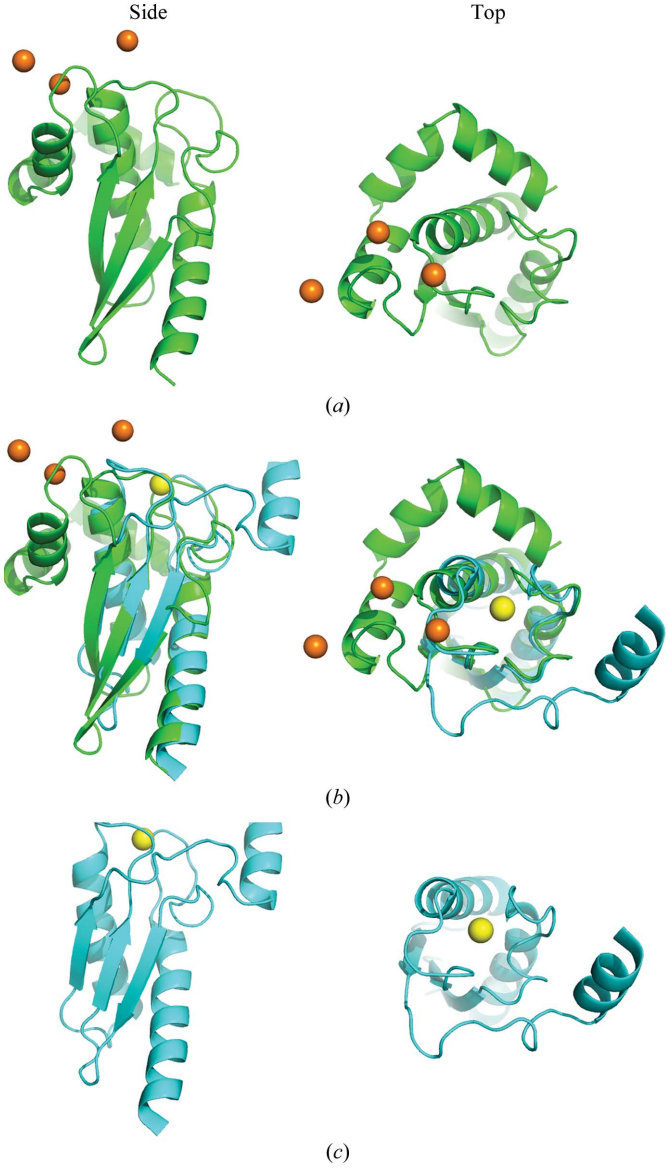

Figure 7
Comparison of the Fam96a monomer model with the bacterial DUF59 protein structure. Left and right views are related by a 90° rotation around the *x* axis. (*a*) Fam96a (green) showing the bound positions of the three zinc ions in orange. The C-terminal region surrounding helix α2 is located at the top left in the left-hand view. (*b*) Superimposition of Fam96a and the bacterial DUF59 structure (PDB entry 3lno). Apart from the C-terminal regions, the core folds overlay well. (*c*) PDB entry 3lno: the predicted metal-binding site is shown in yellow and the position of the C-terminal region is to the right of the core fold in the left-hand view.

We thank Brett Collins for training and assistance with the ITC experiments, Robert Simpson for assistance with the analytical ultracentrifugation data, Katryn Stacey, Jasmyn Dunn and Greg Kelly for providing reagents, Felicia Goh and Allan Burrows for technical assistance, Robert Parton for helpful discussions on localization, Kate Schroeder for helpful discussions on genes enriched in macrophages and Mitchell Guss for helpful discussions on metal coordination. This project was funded by Australian Research Council (ARC) grant DP0770465 to JLM, BK and SK. JLM is an ARC Australian Laureate Fellow and Honorary National Health and Medical Research Council (NHMRC) Research Fellow, BK is an NHMRC Research Fellow and MJS is an ARC Future Fellow and Honorary NHMRC Senior Research Fellow. We acknowledge the use of the University of Queensland Remote Operation Crystallization and X-ray (UQ ROCX) Diffraction Facility and the assistance of Karl Byriel and Gordon King. X-ray data were measured on the MX2 micro-focus beamline at the Australian Synchrotron, Victoria, Australia.

References

Adams, P. D. *et al.* (2010). *Acta Cryst.* D**66**, 213–221.
Almeida, M. S., Herrmann, T., Peti, W., Wilson, I. A. & Wüthrich, K. (2005). *Protein Sci.* **14**, 2880–2886.
Balk, J., Aguilar Netz, D. J., Tepper, K., Pierik, A. J. & Lill, R. (2005). *Mol. Cell. Biol.* **25**, 10833–10841.
Bennett, M. J., Sawaya, M. R. & Eisenberg, D. (2006). *Structure*, **14**, 811–824.
Bergfors, T. (2003). *J. Struct. Biol.* **142**, 66–76.
Chen, V. B., Arendall, W. B., Headd, J. J., Keedy, D. A., Immormino, R. M., Kapral, G. J., Murray, L. W., Richardson, J. S. & Richardson, D. C. (2010). *Acta Cryst.* D**66**, 12–21.
DeLano, W. L. (2002). *PyMOL*. http://www.pymol.org.
Eakin, C. M., Attenello, F. J., Morgan, C. J. & Miranker, A. D. (2004). *Biochemistry*, **43**, 7808–7815.
Edeling, M. A., Guddat, L. W., Fabianek, R. A., Halliday, J. A., Jones, A., Thöny-Meyer, L. & Martin, J. L. (2001). *Acta Cryst.* D**57**, 1293–1295.
Emsley, P. & Cowtan, K. (2004). *Acta Cryst.* D**60**, 2126–2132.
Fan, L., Fuss, J. O., Cheng, Q. J., Arvai, A. S., Hammel, M., Roberts, V. A., Cooper, P. K. & Tainer, J. A. (2008). *Cell*, **133**, 789–800.
Finn, R. D., Tate, J., Mistry, J., Coggill, P. C., Sammut, S. J., Hotz, H. R., Ceric, G., Forslund, K., Eddy, S. R., Sonnhammer, E. L. & Bateman, A. (2008). *Nucleic Acids Res.* **36**, D281–D288.
Holm, L. & Rosenström, P. (2010). *Nucleic Acids Res.* **38**, W545–W549.
Ito, S., Tan, L. J., Andoh, D., Narita, T., Seki, M., Hirano, Y., Narita, K., Kuraoka, I., Hiraoka, Y. & Tanaka, K. (2010). *Mol. Cell*, **39**, 632–640.
Janowski, R., Abrahamson, M., Grubb, A. & Jaskolski, M. (2004). *J. Mol. Biol.* **341**, 151–160.

Janowski, R., Kozak, M., Jankowska, E., Grzonka, Z., Grubb, A., Abrahamson, M. & Jaskolski, M. (2001). *Nature Struct. Biol.* **8**, 316–320.
Joosten, K., Cohen, S. X., Emsley, P., Mooij, W., Lamzin, V. S. & Perrakis, A. (2008). *Acta Cryst.* D**64**, 416–424.
Kabsch, W. (2010). *Acta Cryst.* D**66**, 125–132.
Knaus, K. J., Morillas, M., Swietnicki, W., Malone, M., Surewicz, W. K. & Yee, V. C. (2001). *Nature Struct. Biol.* **8**, 770–774.
Langer, G., Cohen, S. X., Lamzin, V. S. & Perrakis, A. (2008). *Nature Protoc.* **3**, 1171–1179.
Lattin, J. E., Schroder, K., Su, A. I., Walker, J. R., Zhang, J., Wiltshire, T., Saijo, K., Glass, C. K., Hume, D. A., Kellie, S. & Sweet, M. J. (2008). *Immunome Res.* **4**, 5.
Lee, S. & Eisenberg, D. (2003). *Nature Struct. Biol.* **10**, 725–730.
Lezhneva, L., Amann, K. & Meurer, J. (2004). *Plant J.* **37**, 174–185.
Liu, C., Sawaya, M. R. & Eisenberg, D. (2011). *Nature Struct. Mol. Biol.* **18**, 49–55.
Liu, Y. & Eisenberg, D. (2002). *Protein Sci.* **11**, 1285–1299.
Macedo, S., Mitchell, E. P., Romão, C. V., Cooper, S. J., Coelho, R., Liu, M. Y., Xavier, A. V., LeGall, J., Bailey, S., Garner, D. C., Hagen, W. R., Teixeira, M., Carrondo, M. A. & Lindley, P. (2002). *J. Biol. Inorg. Chem.* **7**, 514–525.
Mardones, G. & González, A. (2003). *J. Immunol. Methods*, **275**, 169–177.
McCoy, A. J., Grosse-Kunstleve, R. W., Adams, P. D., Winn, M. D., Storoni, L. C. & Read, R. J. (2007). *J. Appl. Cryst.* **40**, 658–674.
McPhillips, T. M., McPhillips, S. E., Chiu, H.-J., Cohen, A. E., Deacon, A. M., Ellis, P. J., Garman, E., Gonzalez, A., Sauter, N. K., Phizackerley, R. P., Soltis, S. M. & Kuhn, P. (2002). *J. Synchrotron Rad.* **9**, 401–406.
Morris, R. J., Perrakis, A. & Lamzin, V. S. (2003). *Methods Enzymol.* **374**, 229–244.
Nilsson, M., Wang, X., Rodziewicz-Motowidlo, S., Janowski, R., Lindström, V., Onnerfjord, P., Westermark, G., Grzonka, Z., Jaskolski, M. & Grubb, A. (2004). *J. Biol. Chem.* **279**, 24236–24245.
O'Neill, J. W., Manion, M. K., Maguire, B. & Hockenbery, D. M. (2006). *J. Mol. Biol.* **356**, 367–381.
Richards, A. A., Stang, E., Pepperkok, R. & Parton, R. G. (2002). *Mol. Biol. Cell*, **13**, 1750–1764.
Richards, A. A., Stephens, T., Charlton, H. K., Jones, A., Macdonald, G. A., Prins, J. B. & Whitehead, J. P. (2006). *Mol. Endocrinol.* **20**, 1673–1687.
Rual, J. F. *et al.* (2005). *Nature (London)*, **437**, 1173–1178.
Schlunegger, M. P., Bennett, M. J. & Eisenberg, D. (1997). *Adv. Protein Chem.* **50**, 61–122.
Sharma, A. K., Pallesen, L. J., Spang, R. J. & Walden, W. E. (2010). *J. Biol. Chem.* **285**, 26745–26751.
Sheldrick, G. M. (2010). *Acta Cryst.* D**66**, 479–485.
Song, F., Zhuang, Z., Finci, L., Dunaway-Mariano, D., Kniewel, R., Buglino, J. A., Solorzano, V., Wu, J. & Lima, C. D. (2006). *J. Biol. Chem.* **281**, 11028–11038.
Srinivasan, V., Netz, D. J., Webert, H., Mascarenhas, J., Pierik, A. J., Michel, H. & Lill, R. (2007). *Structure*, **15**, 1246–1257.
Stafford, W. F. & Sherwood, P. J. (2004). *Biophys. Chem.* **108**, 231–243.
Staros, J. V. & Anjaneyulu, P. S. (1989). *Methods Enzymol.* **172**, 609–628.
Studier, F. W. (2005). *Protein Expr. Purif.* **41**, 207–234.
Su, A. I., Wiltshire, T., Batalov, S., Lapp, H., Ching, K. A., Block, D., Zhang, J., Soden, R., Hayakawa, M., Kreiman, G., Cooke, M. P., Walker, J. R. & Hogenesch, J. B. (2004). *Proc. Natl Acad. Sci. USA*, **101**, 6062–6067.
Winn, M. D. *et al.* (2011). *Acta Cryst.* D**67**, 235–242.
Wouters, M. A., Fan, S. W. & Haworth, N. L. (2010). *Antioxid. Redox Signal.* **12**, 53–91.
Wu, C., Orozco, C., Boyer, J., Leglise, M., Goodale, J., Batalov, S., Hodge, C. L., Haase, J., Janes, J., Huss, J. W. III & Su, A. I. (2009). *Genome Biol.* **10**, R130.
Wunder, C., Lippincott-Schwartz, J. & Lorenz, H. (2010). *Current Protocols in Cell Biology*, Unit 5.7. doi:10.1002/0471143030.cb0507s49.
Yang, W., Itoh, F., Ohya, H., Kishimoto, F., Tanaka, A., Nakano, N., Itoh, S. & Kato, M. (2011). *Cancer Sci.* **102**, 1808–1814.
Zahn, R., Liu, A., Lührs, T., Riek, R., von Schroetter, C., López García, F., Billeter, M., Calzolai, L., Wider, G. & Wüthrich, K. (2000). *Proc. Natl Acad. Sci. USA*, **97**, 145–150.
Zatta, P., Drago, D., Bolognin, S. & Sensi, S. L. (2009). *Trends Pharmacol. Sci.* **30**, 346–355.
Žerovnik, E., Stoka, V., Mirtič, A., Gunčar, G., Grdadolnik, J., Staniforth, R. A., Turk, D. & Turk, V. (2011). *FEBS J.* **278**, 2263–2282.